IOP Publishing | Royal Swedish Academy of Sciences Physica Scripta

Phys. Scr. **T171** (2020) 014041 (8pp) https://doi.org/10.1088/1402-4896/ab4c29

Multi-physics modeling of the long-term evolution of helium plasma exposed surfaces*

A Lasa[1,4], J M Canik[2], S Blondel[1], T R Younkin[1], D Curreli[3], J Drobny[3], P Roth[2], M Cianciosa[2], W Elwasif[2], D L Green[2] and B D Wirth[1,2]

[1] Nuclear Engineering Department, University of Tennessee, Knoxville, TN, United States of America
[2] Oak Ridge National Laboratory, Oak Ridge, TN, United States of America
[3] Dept. of Nuclear, Plasma, and Radiological Engineering, University of Illinois at Urbana-Champaign, IL, United States of America

E-mail: aesquisa@utk.edu

Received 5 June 2019, revised 23 September 2019
Accepted for publication 8 October 2019
Published 6 March 2020

Abstract

In this manuscript we introduce a simulation tool-suite for predicting plasma-surface interactions (PSI), which aims to predict the evolution of the plasma-facing surfaces that continually change due to exposure to fusion plasmas. A comprehensive description of PSI involves a wide range of physical phenomena, of which we include components for (a) the gas implantation and its dynamic evolution below the divertor surface; (b) erosion of wall material; (c) transport and re-deposition of the eroded impurities; and (d) the scrape-off layer plasma including fuel ions and extrinsic impurities. These components are integrated to predict changes in surface morphology and fuel recycling, and the effect of material erosion and re-deposition in fuel retention. Integrated simulations for ITER-like parameters in a helium plasma environment are presented, focused on the response of the tungsten divertor. The model is also applied to predicting the response of the tungsten surface pre-damaged by He plasma, to burning plasma operations. This case further demonstrates the capability to model the effect of sub-surface helium dynamics, which include helium nucleation, clustering and the bursting of over-pressurized bubbles, its impact on fuel recycling as well as the effect of sputtering on the surface evolution.

Keywords: plasma surface interactions, helium, plasma sheath, impurity transport, tungsten

(Some figures may appear in colour only in the online journal)

1. Introduction

The interfacial region where the edge plasma meets the material poses numerous scientific challenges for the viability of fusion power. This interaction region couples the boundary and scrape off layer (SOL) plasma to the near surface materials via the plasma sheath. The plasma-facing components (PFCs) respond to and feed back on the SOL, characterized by the extreme thermal and particle fluxes. Further, these plasma-surface interactions (PSI) are time varying as a result of the local plasma conditions and changes in material surface properties due to both gas implantation and exposure to a 14 MeV peaked neutron spectrum. Understanding and controlling these interlinked interactions is widely recognized as a critical need for the realization of commercial fusion power [1], because these interactions determine: (1) the PFC lifetime due to erosion, (2) core plasma fusion performance through

[4] Author to whom any correspondence should be addressed.

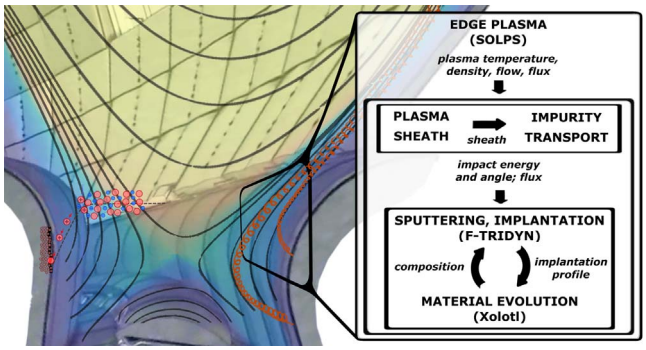

Figure 1. Schematic illustration of a tokamak divertor, outlining the magnetic field line structure, plasma density (gradient), sputtered impurity trajectories (orange) and potential drop at the sheath for ions (red) and electrons (blue); next to the code-coupling workflow to model PFC surface evolution. The sketched features (sheath, trajectories, divertor plates, etc) are not to scale.

recycling of hydrogenic species and contamination by eroded impurities, and (3) tritium (T) management, including (co-) deposition of T in eroded/re-deposited material.

Here we describe the integration of multiple boundary and material models within a simulation capability that addresses PSI (section 2), including the modification of the plasma facing surface layer due to contact with the fusion plasma. PSI involves a wide range of physical phenomena, of which our current model includes components for (a) the scrape-off layer plasma including impurities and fuel ions (sections 2.1 and 2.2), (b) wall erosion, and transport and re-deposition of the eroded impurities (sections 2.3 and 2.4), (c) the implantation of plasma species (gases and impurities) into the wall material (section 2.4), and (d) the gas dynamics in the subsurface (section 2.5). These components are used to predict material erosion and changes in surface morphology, fuel recycling and retention, and the effect of material erosion and re-deposition on fuel retention. We apply this simulation capability to the study of the modification of the ITER W divertor exposed to He plasmas (section 3), and evaluate the impact of the He exposure in fuel recycling during subsequent deuterium-tritium plasmas (section 4).

2. Integrated modeling of PSI

The integrated model contains a wide range of effects that are coupled under several constraints as illustrated schematically in figure 1. This includes models for the background plasma transport (using the SOLPS code [2]), the near-surface sheath effects (with hPIC [3]), the erosion and transport of wall material across SOL (in GITR [4]), sputtering by and implantation of ions impacting on the material (in F-TRIDYN [5]), and the dynamics of the subsurface gas atoms (with Xolotl [6]). Each of these codes is described briefly below and in greater detail in the literature [7, 8]. At present, steady-state plasma conditions are considered, with a one-way coupling that passes information from the plasma to the materials models to evolve the surface, as sketched in figure 1.

2.1. SOLPS modeling of divertor plasma conditions

The SOLPS code package models the conditions in the scrape-off layer: the B2.5 code [9] models the plasma, using a 2D fluid description, and neutral particle transport is calculated via coupling to the kinetic Monte Carlo code EIRENE [10]. The model includes parallel and cross-field transport of plasma and neutrals, and ionization, recombination, charge-exchange, and line radiation. For a given set of core plasma conditions (e.g. input power and density at the separatrix), SOLPS calculates the 2D distribution of density and temperature of all charge states, including the plasma in contact with the divertor surfaces and the heat and particle fluxes onto those surfaces. SOLPS has already been used for predictive modeling of the ITER plasmas. The SOLPS-ITER version [11] is used in the present work.

2.2. hPIC modeling of the near-surface sheath

The plasma conditions provided by SOLPS are passed as an input to the hPIC code. hPIC is a full-f, full-orbit particle-in-Cell (PIC) code resolving the plasma sheath physics. Of interest to this workflow, it provides the ion energy-angle distribution (IEAD) of the particles striking the wall. Each hPIC simulation is performed in a 1D3V electrostatic mode, resolving a region of approximately 500 Debye lengths along the normal to the surface, using an average of 1000 particles per cell, 5 grid points per Debye length and 50 time steps per ion gyro-period.

2.3. GITR modeling of the transport and deposition of eroded wall material

The global impurity transport code (GITR) models the ionization, transport and re-deposition of eroded wall material, including both prompt re-deposition and long-range transport controlling global deposition, in realistically detailed 3D PFC surfaces over large regions of the SOL. GITR uses input data for the magnetic field, background plasma profiles, sheath characteristics, and PFC surfaces, which are then used to simulate the trajectories of eroded particles ejected from the surface. The physical model includes the Lorentz Force (including $E \times B$ and ∇B particle drifts), Monte Carlo operators for atomic physics (ionization, recombination), interaction with the background plasma (Coulomb collision effects, including the thermal force), anomalous cross-field diffusion, and interactions with material surfaces (energy and angle dependent sputtering and reflection yields). This approach relies on a trace impurity approximation to track the tungsten (W) eroded from the surface. From a computer science perspective, this means solving many parallel ODEs (trace impurity particle trajectories) with a set of Monte Carlo operators with time steps of $\sim$1 ns. To model times of O(ms) to O(s) necessary to resolve long range transport, and to achieve statistically significant results, the codes typically resolves O(10^6)–O(10^9) times steps for O(10^6)–O(10^8) particles.

2.4. F-TRIDYN modeling of sputtering and implantation of plasma ions

The yield and energy-angular distribution of sputtered particles (used by GITR), as well as ion implantation profiles (needed for Xolotl) are calculated by the binary collision code Fractal (F)-TRIDYN. F-TRIDYN is a version of the ion-solid interaction code TRIDYN [12] upgraded to include a robust fractal model of surface morphology. The code resolves the physics of surface erosion and particle implantation, producing relevant quantities such as sputtering yields, energy-angle distribution of the emitted particles (sputtered impurities, reflected recoils, and pre- implanted gas), reflection and backscattering coefficients, and Frenkel pair production.

2.5. Xolotl modeling of surface evolution

The Xolotl code models the sub-surface evolution of gas species implanted into the tungsten divertor tiles, along with associated changes in surface height. Xolotl is a continuum-based cluster dynamics code solving the spatially dependent drift-diffusion-reaction (DDR) equations in one to three spatial dimensions (1D–3D) to predict the evolution of the concentration fields for a mixed helium-hydrogen implanted tungsten material. It can simulate time scales of 100–1000 s and length scales of nm-mm. The clusters under consideration consist of six types: tungsten self-interstitials (I), tungsten vacancies (V), helium (He), deuterium (D), tritium (T), and trapped defect-vacancy clusters (He-D-T-V). The parameters needed in the DDR equations are obtained from other methods: F-TRIDYN simulations provide the distribution of implanted gas atoms, while the diffusion parameters, interaction radii governing reactions and formation/binding energies are obtained from atomistic (Density Functional Theory and Molecular Dynamics) modeling [13, 14].

Xolotl includes a model for surface growth based on observations of atomistic simulations: self-interstitial tungsten atoms created during trap mutation reactions are highly mobile and reach the surface, where they deposit as adatoms, eventually accumulating to generate new layers of material. This is represented in Xolotl by a grid that extends beyond the initial surface position. When the number of tungsten self-interstitial atoms that diffuse to the surface exceeds the density of tungsten, the surface position is moved outward. Re-deposition of tungsten is also modeled as a flux of tungsten self-interstitial atoms that are implanted on (or slightly below) the surface to form additional adatoms. Sputtering of tungsten by plasma ions is also included as a mechanism for the surface to recede. Finally, a bubble bursting model has been introduced to mimic the release of gas from over-pressured bubbles, as described in [15], where the near-surface bubbles are able to free their content (helium-hydrogen) to form a cavity that can be filled by incoming fluxes.

2.6. Integrated workflow for modeling the plasma-material interface

These codes are coupled using the integrated plasma simulation (IPS) framework. IPS [16] is a high-performance computing framework developed with focus on flexibility for loosely-coupled, component-based simulations, providing services to manage resources and data, and to execute, coordinate and communicate between components. At the outermost level, SOLPS resolves the fluid background plasma. Using these profiles as input hPIC, calculates the impact energy-angle distributions for each species in the background plasma. These distributions provide input to GITR, together with a reduced model for particle sputtering and reflection calculated by F-TRIDYN, to resolve the W sputtering and re-deposition. The angle and energy-dependent incident ion flux provided by hPIC (for the main plasma species) and by GITR (for re-deposited tungsten), is input to the coupled Xolotl and F-TRIDYN models to predict the sub-surface gas dynamics and material evolution. F-TRIDYN provides the implantation profiles of the incident plasma ions and effective sputtering yields to Xolotl, and Xolotl in turn models the evolving surface composition, with an iteration between the two codes since composition impacts both sputtering and implantation depth. The end result is a simulation capability to model the dynamics of gas species within the divertor sub-surface, the motion of the surface, and gas recycling and retention, including the effects of erosion and re-deposited layers on the PFC surface. In general, inputs received from components in the workflow act as common boundary conditions. Studying the sensitivity and correlations of other boundary conditions (i.e. not defined by outputs of the integrated model, such as the sheath heat transmission factor used in SOLPS and that output by hPIC later on for the same plasma conditions) is beyond the scope of the current paper. Such sensitivity studies can be found in the literature for cases similar to the example mentioned above [17].

3. Effects of helium on plasma exposed tungsten

The ITER research plan currently includes an operational phase using helium plasmas before the full burning plasma phase. The response of tungsten PFCs to helium plasmas is of special interest due to the profound impact that He exposure can have on the surface integrity, most dramatically illustrated by the observed growth of tungsten 'fuzz' [18]. While direct simulation of fuzz growth is not targeted here, He plasma exposures are useful for studying the dynamics of gas within the W surface and the evolving surface morphology with some experimental trends already accessible.

3.1. Simulations of PSI during ITER helium plasma operation

The background plasma for the ITER helium case is simulated by SOLPS, with an input power of 40 MW, representative of the planned early ITER operation. The transport was fixed as spatially constant, with values for the particle and electron/ion thermal diffusivities of $D = 0.3$ and $\chi_e = \chi_i = 1.0\,m^2\,s^{-1}$; these represent the standard values for ITER SOLPS simulations and produce SOL solutions that have been well-documented [19, 20]. The plasma is predominantly He, with ~5% hydrogen (H) content included to

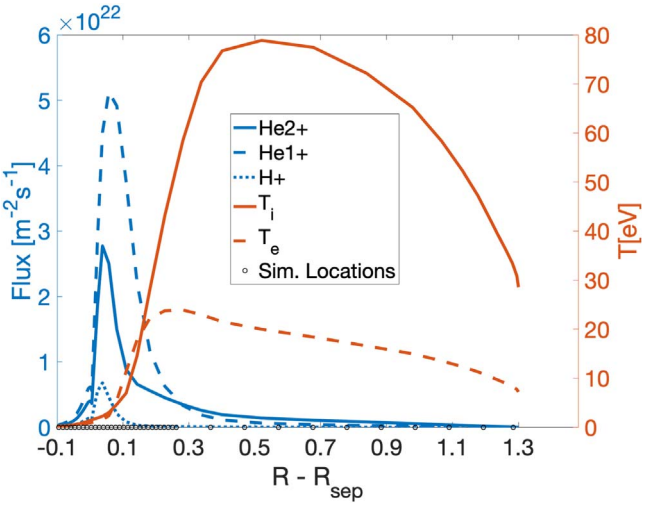

Figure 2. Plasma flux and temperature profiles along the outer divertor target, as calculated by SOLPS.

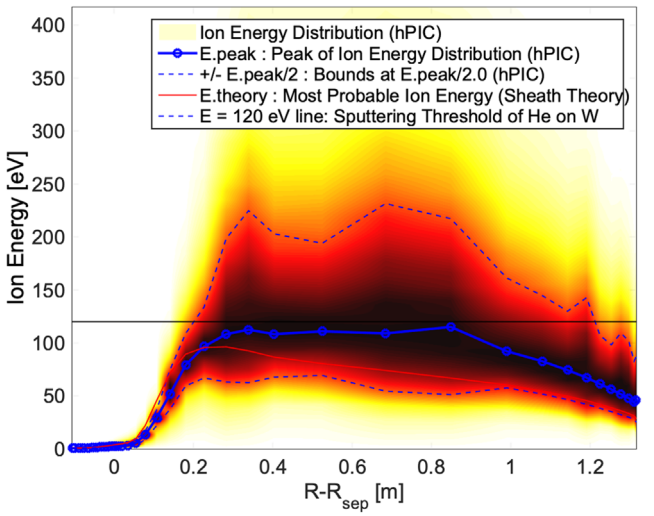

Figure 3. Ion energy distribution integrated over the angular dimension along the outer targer ($R- R_{sep}$) predicted by hPIC for He^+. The sputtering threshold of W by He (dashed blue line) is given for normal incidence.

account for residual H present in the system (potentially due to pellet fuelling). Realistic pumping in the divertor is included, and the plasma is fuelled by edge gas puffing set to a level that produces a mid-plane separatrix density of $n_e \sim 1.5 \times 10^{19}\,m^{-3}$.

Strong radiation is predicted for the helium scenarios under these conditions. SOLPS calculates that 25 MW of the 40 MW input power is radiated, with nearly the entirety being localized in the divertor region and with only modest differences between the inner and outer leg. Figure 2 presents the plasma profiles of the partially detached divertor consisting of the ion and electron temperatures (red) and fluxes (blue). The output indicates a very low temperature (~eV) near the strike point indicative of a local detached plasma, and radially increasing electron and ion temperatures into the ~20 eV and ~80 eV range (respectively) farther along the SOL where the plasma remains attached. The electron density (not shown in figure 2) is highest near the strike point, reaching relatively modest values of $\sim 4 \times 10^{20}\,m^{-3}$ in this low power scenario. Likewise the total ion flux is high near the strike point, and both density and ion flux decrease significantly farther along the SOL.

At each point on the SOLPS grid at the outer target—a total of 38 points—an hPIC simulation is performed based on the local magnetic field angle of incidence and SOLPS plasma parameters (e.g. the initial velocity of ions is set to a Maxwellian distribution for the local ion temperature). In these simulations (as well as the subsequent workflow), the focus is on the helium behavior, and thus hydrogen has been neglected due to the low concentration and low energies that will not contribute to erosion. An hPIC simulation was performed for both He^+ and He^{++} plasmas up to steady state. The characteristics of ions hitting the wall were recorded to produce the energy distribution (i.e. integral of the IEAD over the angles) as a function of the geometrical coordinate $R - R_{sep}$ along the ITER outer target, as summarized in figure 3 for He^+. A black horizontal line marks the sputtering threshold of helium on tungsten (119.95 eV). For light ions and low ionization states, while the peak of the distribution generally falls below the sputtering threshold, a portion of the high-energy tail is above this limit and contributes to sputtering. This is illustrated in figure 3 for He^+ ions and highlights the relevance of resolving the IEADs (e.g. here calculated by hPIC). In the He^{++} case (not shown here), the peak of the distribution is above the sputtering threshold up to ~0.5 m from the strike point. With the IEAD calculated by hPIC, the F-TRIDYN and GITR codes perform a quantitative analysis of gross and net erosion, as described in the next section.

Based on the background plasma data (SOLPS plasma profiles and IEADs of He at the outer divertor target), F-TRIDYN calculates the initial conditions (sputtering and reflection yields) to provide the He sputtered W source to GITR. GITR simulates 10^6 particles to represent the erosion and migration of the tungsten impurities for a duration of 2 ms, which provide sufficient statistics and time duration to capture the prompt re-deposition as well as transport of impurities in the SOL. The results of the impurity transport simulation show slightly higher gross erosion, relative to gross deposition flux resulting in net erosion along the ITER outer divertor target over a distance of approximately 90 cm in the positive $R - R_{sep}$ coordinate (figure 4(a)). The shape of this erosion profile mimics the erosion profile from the background He^+ and He^{++} plasma fluxes. In these simulations approximately 80% of the eroded tungsten is redeposited while 20% is lost to a combination of the private flux region, scrape-off layer, or surface locations further away from the outer divertor target. He^{++} is the dominant erosion source followed by He^+ and then the self-erosion caused by sputtered, ionized and re-deposited W.

The coupled model of F-TRIDYN and Xolotl also calculates the surface growth and erosion along the target,

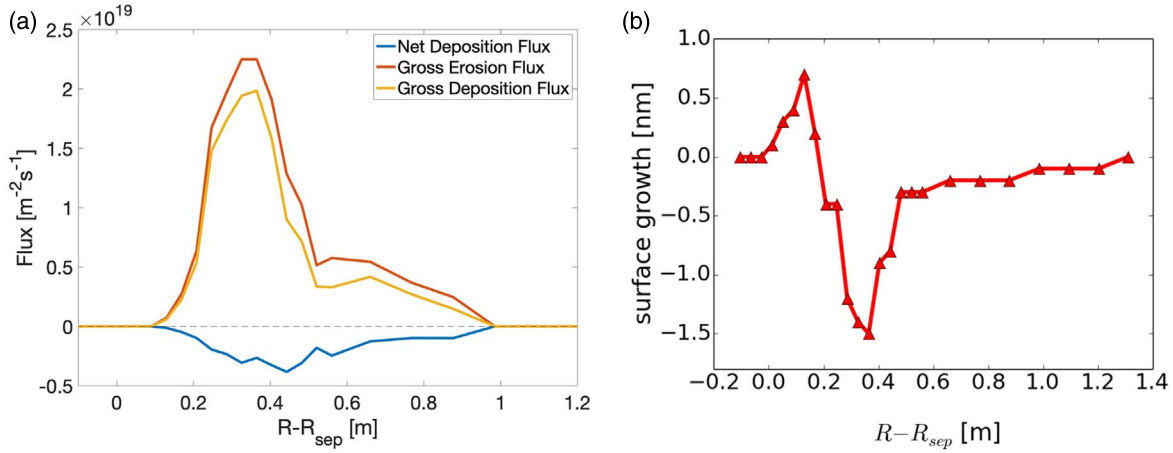

Figure 4. (a) Tungsten gross erosion, gross deposition and net deposition fluxes calculated by GITR, and (b) net changes in surface height predicted by Xolotl, which additionally accounts for the effect of sub-surface gas dynamics; along the outer divertor. Negative values represent net erosion and positive values indicate deposition or growth.

(figure 4(b)). In addition to W sputtering and re-deposition, the model accounts for the contribution of the sub-surface gas dynamics (retention and clustering) to surface growth, and reflects the complex interplay between plasma flux and plasma temperature. In the private flux region ($R - R_{\rm sep} < 0$) both plasma flux and temperature are small, leading to no significant He implantation or surface erosion. As the He plasma flux increases near the strike point, the models predict a surface growth peak due to helium implantation below the surface leading to helium bubble nucleation and the concomitant trap mutation, loop punching and tungsten self-interstitial migration to the surface, resulting in extensive adatom formation. In this region, the plasma temperature and thus helium ion impact energy are low and sputtering yields are small such that there is essentially no erosion. Further beyond the strike point ($R - R_{\rm sep} > 0.2$ m), the flux decreases and the plasma temperature increases, resulting in lower gas implantation fluxes, but higher ion temperatures that produce higher sputtering yields. Thus, the surface transitions from net surface growth to net erosion and mimics the trend in GITR.

He retention as simulated by Xolotl and defined relative to the implanted flux, is largest for the plasma conditions with peak plasma temperature which results in deeper gas implantation, although the total accumulated helium inventory in the tungsten divertor is dominated by the regions with higher implantation flux. The predicted helium concentrations following the 10 s discharge (figure 5(a)) indicate higher helium concentrations at the locations of higher implantation flux, with values increasing from about 75 ppm at the peak flux location to a maximum value of about 390 ppm at $R- R_{\rm sep} = 0.2$ m, and then decreasing sharply as the implantation flux decreases.

Figure 5(b) compares the time dependent helium retention in the tungsten divertor at the positions of peak flux (orange) versus peak plasma temperature (blue). While the relative retention is higher for the peak plasma temperature location, the implantation flux is about an order of magnitude lower, and thus the helium concentration is only about 40 ppm compared to ∼75 ppm at the peak flux location. Figure 5(b) also shows significant oscillations in helium retention, which result from the bursting of sub-surface helium bubbles that release He. Since small clusters (bubbles) created near the surface can easily burst, deeper ion implantation (resulting from higher plasma temperature) is more efficient at increasing the retention than increases in flux. At the location of the highest plasma temperature, we observe that Xolotl predicts less frequent but larger helium bubble bursting events, as helium ions implant deeper and the flux is relatively low, allowing He to diffuse deeper prior to bubble nucleation and growth. In contrast, near the strike point (around the peak in flux), He is implanted closer to the surface and at a higher rate, producing relatively quick helium self-clustering and thus more frequent but smaller bursting events, as indicated by figure 5(b).

As shown in figure 5(c), the different plasma flux and temperatures lead to very different cluster size distributions at the peak plasma flux (orange) as compared to the location of peak plasma temperature (blue). Bubble nucleation results from the self clustering interaction of two He atoms, which then further grow by absorbing He and undergoing trap mutation, which creates a Frenkel pair with the vacancy immobilizing the cluster. Under high flux condition, He ions are implanted close to the surface, leading to rapid nucleation and growth of clusters, which tend to burst as the clusters grow to intermediate sizes within the near surface (<50 nm depth) region. However, a more detailed look at the depth dependent size distribution in figure 5(c), indicates that the frequent bubble bursting events actually reduce the concentration of clusters with size from about 10 to 50 relative to those formed at the peak surface temperature locations. Finally, the peak in helium concentration at a cluster size of 200 (maximum size tracked here) is an artifact of the reaction network size chosen for the simulations, and indicates that

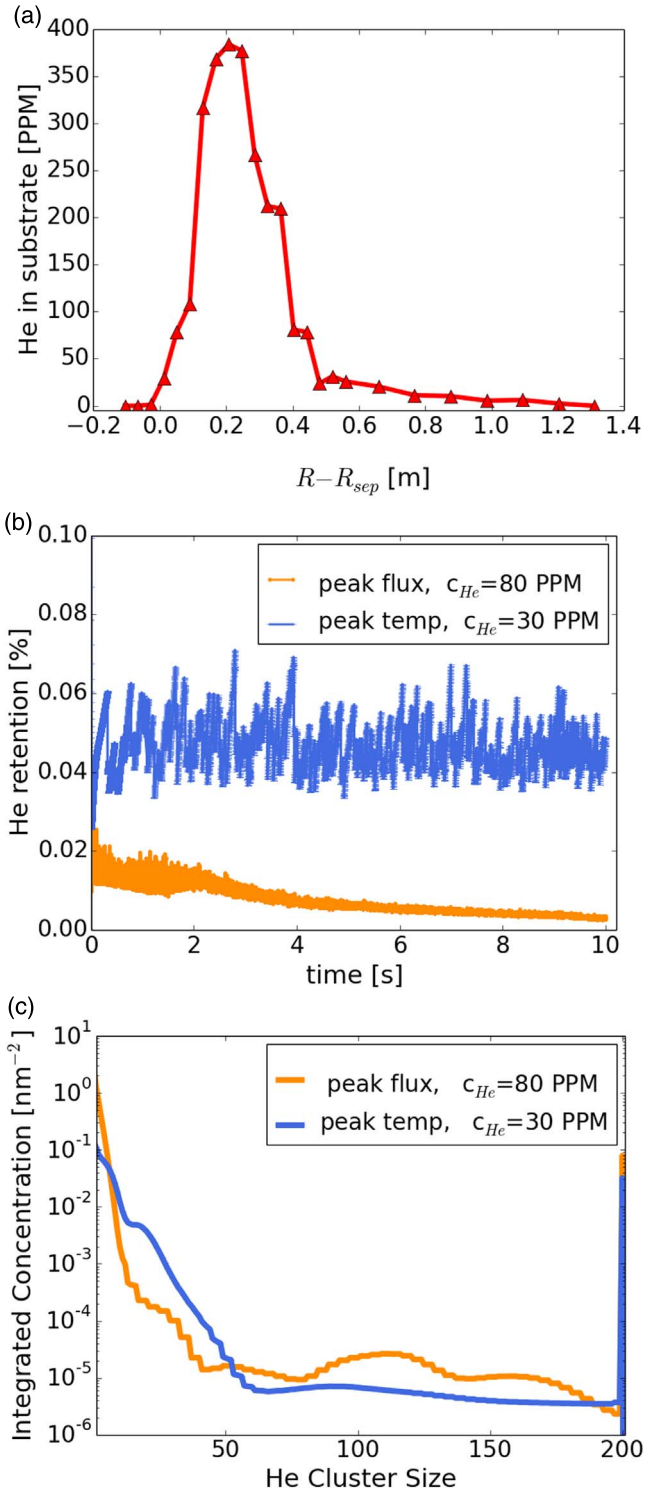

Figure 5. Xolotl predictions of (a) Depth-integrated He content below the W surface along the outer divertor; and (b) time-dependent percentage of retained helium fraction (relative to implanted), and (c) depth integrated helium concentration as a function of helium cluster size, near the peak plasma temperature (blue) and peak flux (orange), with the He content (c_{He}) of these two locations given for reference.

larger clusters will form. However, we do not expect this would modify the conclusions regarding the relative retention and cluster size distribution variations, although we do expect a larger average He cluster size.

3.2. BPO on a pre-damaged substrate

We have also modeled the exposure of a W target damaged by 10 s of He plasma, to conditions expected during burning D-T-He plasma operations (BPO), and compared the output to a crystalline W divertor exposed only to BPO. The modeling of the BPOS conditions follows the workflow described ealier, but the integrated simulations now incorporate a much larger set of species with the addition of D, T and neon (Ne). Further, Xolotl also incorporates the plasma heat flux to the W divertor as input to solve the 1D thermal diffusion equation and calculate the resulting temperature distribution in the target. These BPO simulations modeled the divertor surface evolution for O(10) s. These simulations are described in detail in [7, 8].

As an illustrative example, figure 6 presents the output for a location with peak plasma temperature during BPO ($R - R_{\mathrm{sep}} \sim 0.11$ m; $T_{\mathrm{i}} \sim 42$ eV; $\Gamma \sim 8{\cdot}10^{22}$ ion m^{-2} s^{-1}). The helium depth profiles clearly indicate that the He concentration is significantly higher (by over 1000×) in the substrate with pre-implanted He (figure 6(b)) than in the initially pristine W substrate (figure 6(a)). This is expected from the large He fluence accumulated during the 10 s He plasma exposure ($3{\cdot}10^{23}$ He m^{-2}), compared with the small He fraction in the D-T-He plasma. The distinctive near-surface peaks due to He clustering (figure insets), visible in both cases, are significantly more prominent and reach deeper depths in the case of a pre-damaged W substrate, especially in the beginning of the BPO. During exposure of the pre-damaged substrate to the D-T-He plasma, the pre-existing high pressure helium bubbles burst, leaving empty vacancies (voids) that quickly fill with the implanted species, in this case, mainly D and T. As a result, the near-surface concentration of He (figure 6(b) inset) decreases during the D-T-He exposure, while that of T (figure 6(d)) increases, by nearly 10× compared to the initially pristine W substrate (figure 6(c)). Likewise, the near-surface concentration peak does not decrease with increasing time despite changes in surface temperature, since these hydrogenic species are more strongly trapped at helium-vacancy and vacancy clusters with de-trapping energies that range from about 1.1 to in excess of 1.5 eV, as predicted by first principles density functional theory calculations [21]. Finally, we observe that the near surface helium cluster microstructure is predicted to reduce the deeper permeation of T and D (figure 6(d), compared to figure 6(c)), at least for the fluences reported here.

4. Summary

This article presents the initial results of an integrated simulation capability for multi-physics modeling of PSI. This is a coupled model that includes descriptions for the background edge plasma, near-surface sheath, erosion and re-deposition, and the evolution of the material surface including the dynamics of sub-surface implanted gas species. Here we apply the model to predicting the response of the ITER divertor PFC surface to He plasma operation, thus

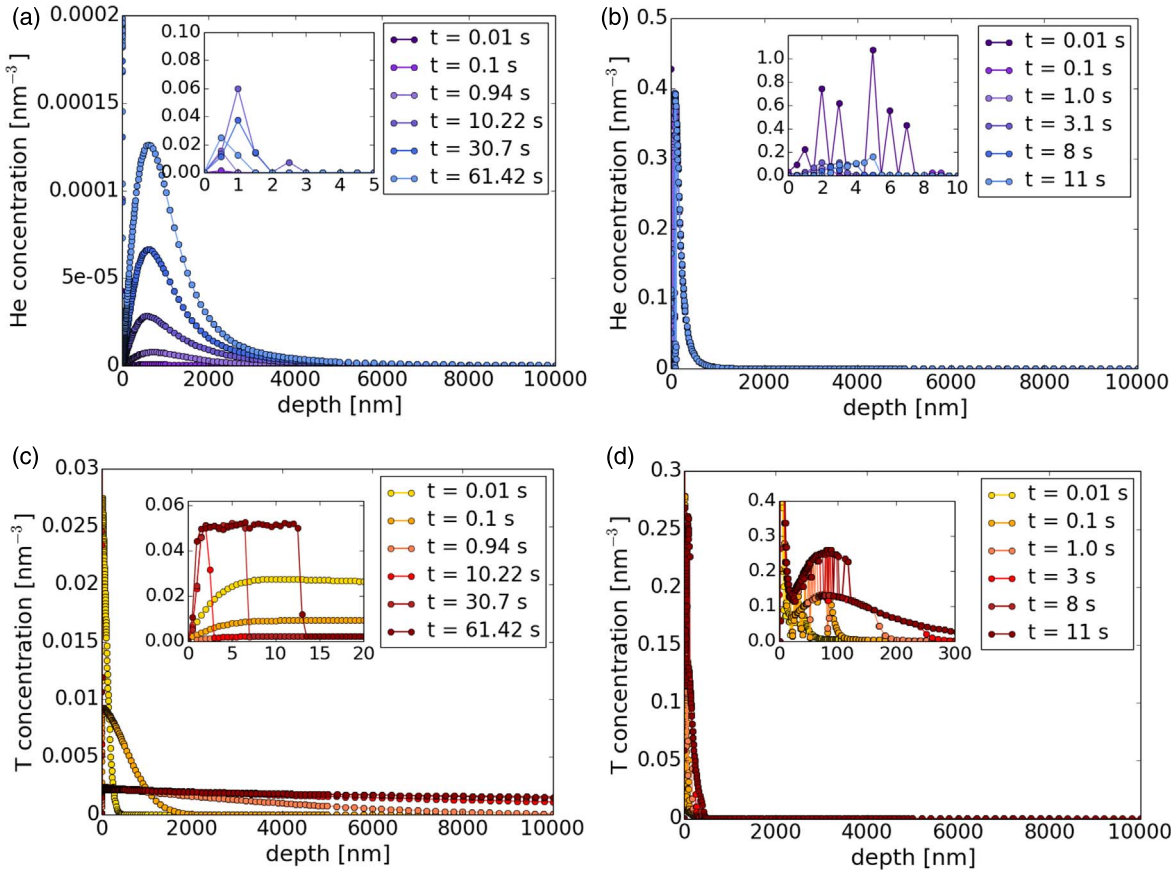

Figure 6. Depth profiles of the cluster-size integrated gas concentrations (in units of atoms nm^{-3}) up to depths of 10 microns, as a function of time at the spatial location of peak plasma temperature ($R - R_{sep} \sim 0.11$ m) for (a) He in pristine W, (b) He in pre-damaged W, (c) T in pristine W and (d) T in pre-damaged W. The insets highlight the concentration profiles in the near surface (5 nm for He, or 100 nm for T).

predicting the He recycling and retention, as well as changes in surface morphology. The SOLPS output predicts a partially detached He plasma. Under these conditions, the sheath effects result in a significant contribution of light ions to sputtering of W due to the high-energy tail of the IEAD. Using the IEAD from hPIC, impurity transport calculations by GITR predict a high (∼80%) local W re-deposition, with net erosion across most of the outer target. When including the effect of sub-surface gases on surface growth, the coupled FTRIDYN-Xolotl simulations predict net surface growth around the strike point instead, along with an extended region of net erosion. Further, Xolotl predicts that He retention (relative to the implanted flux) increases with plasma temperature, although the total sub-surface He content is dominated by He flux. Finally, during exposure to burning D-T plasma conditions, samples pre-damaged by He plasma show higher near-surface concentrations of D-T, but lower hydrogen permeation into the bulk, compared to an initially pristine W target.

Future efforts will expand our code integration effort to account for the feedback onto the boundary plasma in response to changing surface properties and dynamic recycling. Our work will also focus on extending the comparison to tokamak experiments.

Acknowledgments

This project is part of the Scientific Discovery through Advanced Computing (SciDAC) program, and is jointly sponsored by the Fusion Energy Sciences (FES) and Advanced Scientific Computing Research (ASCR) programs within the US Department of Energy, Office of Science. Research supported by the US Department of Energy under DE-AC05-00OR22725.

ORCID iDs

A Lasa https://orcid.org/0000-0002-6435-1884
J Drobny https://orcid.org/0000-0002-9733-6058
M Cianciosa https://orcid.org/0000-0001-6211-5311
B D Wirth https://orcid.org/0000-0002-0395-0285

References

[1] Maingi R 2015 Fusion energy sciences workshop on plasma material interactions: report on science challenges and research opportunities in plasma material interactions (Princeton, NJ: Princeton Plasma Physics Laboratory)

(https://science.osti.gov/-/media/fes/pdf/workshop-reports/2016/PMI_fullreport_21Aug2015.pdf)
[2] Schneidr R *et al* 2006 *Contrib. Plasma Phys.* **46** 3
[3] Khaziev R and Curreli D 2015 *Phys. Plasmas* **22** 043503
[4] Younkin T *et al* 2019 GITR: an accelerated global scale particle tracking code for wall material erosion and redistribution in fusion relevant plasma-material interactions *Comput. Phys. Commun.* submitted
[5] Drobny J *et al* 2017 *J. Nucl. Mater.* **494** 278–83
[6] Blondel S *et al* 2017 *Fusion Sci. Technol.* **71** 22–5
[7] Wirth B D 2018 Final report of the 2018 Theory and Simulation Performance Target on Plasma Materials Interaction *DOE-FES Report* (Washington, DC: DOE-FES) (https://science.osti.gov/fes/community-resources/)
[8] Lasa A *et al* 2019 Integrated plasma-material modeling of the evolution of tungsten divertor surfaces during He and burning plasma discharges in ITER *Nucl. Fusion* submitted
[9] Braams B 1996 *Contrib. Plasma Phys.* **36** 276
[10] Reiter D, Baelmans M and Borner P 2005 *Fusion Sci. Technol.* **47** 172
[11] Wiesen S *et al* 2015 *J. Nucl. Mater.* **463** 480–4
[12] Miller W *et al* 1988 *Comput. Phys. Commun.* **51** 355
[13] Blondel S *et al* 2018 *Nucl. Fusion* **58** 126034
[14] Yang L, Bergstrom Z J and Wirth B D 2018 *J. Appl. Phys.* **123** 205108
[15] Hammond K D, Blondel S, Hu L, Maroudas D and Wirth B D 2018 *Acta Mater.* **144** 561–78
[16] Elwasif W R *et al* 2010 *18th Euromicro Conference on Parallel, Distributed and Network-based Processing* 2010 *(Pisa)* pp 419–27
[17] Canik J M and Tang X-Z 2017 *Fusion Sci. Technol.* **71** 103–9
[18] Doerner R P 2012 *Nucl. Fusion* **52** 103003
[19] Kukushkin A S *et al* 2002 *Nucl. Fusion* **42** 187
[20] Kukushkin A S *et al* 2009 *Nucl. Fusion* **49** 075008
[21] Yang L and Wirth B D 2018 *J. Appl. Phys.* **123** 215104